Solitary Waves and Undular Bores in a Mesosphere Duct

ROGER GRIMSHAW

Department of Mathematical Sciences, Loughborough University, Loughborough, Leicestershire, United Kingdom

DAVE BROUTMAN

Computational Physics, Inc., Springfield, Virginia

BRIAN LAUGHMAN

GATS/Boulder, Inc., Boulder, Colorado

STEPHEN D. ECKERMANN

Space Science Division, Naval Research Laboratory, Washington, D.C.

(Manuscript received 1 December 2014, in final form 29 May 2015)

ABSTRACT

Mesospheric bores have been observed and measured in the mesopause region near 100-km altitude, where they propagate horizontally along a duct of relatively strong density stratification. Here, a weakly nonlinear theory is developed for the description of these mesospheric bores. It extends previous theories by allowing internal gravity wave radiation from the duct into the surrounding stratified regions, which are formally assumed to be weakly stratified. The radiation away from the duct is expected to be important for bore energetics. The theory is compared with a numerical simulation of the full Navier–Stokes equations in the Boussinesq approximation. Two initial conditions are considered. The first is a solitary wave solution that would propagate without change of form if the region outside the duct were unstratified. The second is a sinusoid that evolves into an undular bore. The main conclusion is that, while solitary waves and undular bores decay by radiation from the duct, they can survive as significant structures over sufficiently long periods (~100 min) to be observable.

1. Introduction

Nonlinear internal gravity waves and undular bores in the atmosphere have been intensively studied over several decades; see, for instance, the reviews by Smith (1988) and Rottman and Grimshaw (2001). But only in the last couple of decades have there been analogous observations and consequent theoretical studies in the mesosphere. For instance, Dewan and Picard (1998, 2001) drew attention to a "spectacular gravity wave event" at a height of around 85 km observed from Hawaii as reported by Taylor et al. (1995), and they identified it as a mesospheric bore. This was followed by several other similar observations, notably over Colorado by She et al. (2004); over Antarctica by Nielsen et al. (2006), Bageston et al. (2011), and Stockwell et al. (2011); over northern China by Li et al. (2013); and over the southwestern United States by Smith et al. (2003).

There have been several theoretical presentations reported, essentially based on the concept of wave trapping in a mesosphere duct, and consequent nonlinear evolution exploiting extant theories of undular bores in the context of the nonlinear shallow water equations (e.g., Dewan and Picard 1998, 2001; Snively and Pasko 2003; Seyler 2005). The studies by Laughman et al. (2009, 2011) combined full numerical simulations with an application of a Benjamin–Davis–Acrivos–Ono (BDAO) model, sometimes referred to as the BDO or BO model. The BDAO equation was developed in the pioneering work of Benjamin (1967) and Davis and Acrivos (1967) for the description of internal

Corresponding author address: Roger Grimshaw, Department of Mathematical Sciences, Loughborough University, Loughborough, Leicestershire LE11 3TU, United Kingdom.
E-mail: R.H.J.Grimshaw@lboro.ac.uk

DOI: 10.1175/JAS-D-14-0351.1

Publisher's Note: This article was revised on 29 January 2016 to include an addition to the Acknowledgements section.

solitary waves riding on a shallow stratified layer beneath a deep homogeneous layer. The application by Laughman et al. (2009, 2011) requires extension to a stratified duct embedded between two deep homogeneous layers. Here, we extend that model to include weak stratification in the adjoining deep layers, which then allows for internal gravity waves to be emitted from the duct by the nonlinear waves propagating along the duct. We also consider more general initial conditions and in particular those that lead to the formation of undular bores.

In section 2, we present a derivation of an extended BDAO model, together with an estimate of the decay rate of an internal solitary wave propagating along the duct because of the emission of outwardly propagating internal gravity waves. Then, in section 3, we describe the numerical methods used for the BDAO equation and for some analogous simulations of the full Navier–Stokes equations, followed by some preliminary numerical results in section 4. We conclude in section 5.

2. Theoretical model

a. Derivation

We consider a two-dimensional duct with strong stratification, embedded between two deep layers with weak stratification, extending the derivation of Grimshaw (1981a), which was for a shallow layer beneath a deep layer. For simplicity, we assume also that the deep layers have uniform but weak stratification and that there is no background wind. Some effects of background winds for ducted waves and bores near the mesopause are considered in Fechine et al. (2009), Bageston et al. (2011), and Snively et al. (2007). Further, also for simplicity and for compatibility with the fully nonlinear numerical simulations, we assume incompressible flow. Although this assumption applies in situations when the vertical displacements are much smaller than the density scale height, the present model could be extended to remedy this and take some account of compressibility while still excluding acoustic waves, for instance, as in Grimshaw (1981b), or by replacing the incompressible condition with an anelastic approximation (e.g., Durran and Arakawa 2007; Sutherland 2010; Vallis 2006).

First, we consider the linearized equations for an incompressible fluid [Sutherland 2010, section 3.7.1, their Eq. (3.161)]:

$$\overline{\rho}u_t + p_x = 0, \tag{1}$$

$$\overline{\rho}w_t + p_z + g\rho = 0, \tag{2}$$

$$\rho_t + \overline{\rho}_z w = 0, \quad \text{and} \tag{3}$$

$$u_x + w_z = 0. \tag{4}$$

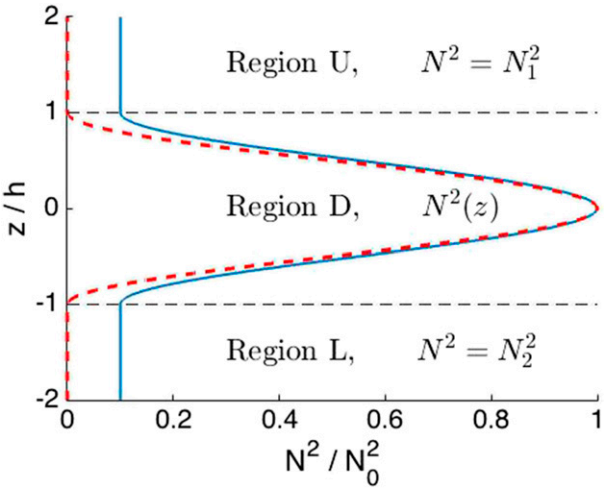

FIG. 1. The model geometry, showing region D in the duct, region U above the duct, and region L below the duct. Two profiles for N^2 are plotted: $N_1^2 = N_2^2 = 0$ (dashed red) and $N_1^2 = N_2^2 = 0.1\ N_0^2$ (solid blue).

Here, the velocity is (u, w) in spatial coordinates (x, z), p is the perturbation pressure, g is gravity, $\overline{\rho}(z)$ is the background density, and ρ is the perturbation density. In the Boussinesq approximation, $\overline{\rho}(z)$ in Eqs. (1) and (2) is replaced with a constant density ρ_0.

We then define the streamfunction ψ such that $(u, w) = (\psi_z, -\psi_x)$. From Eqs. (1)–(4), it can be shown that

$$[(\overline{\rho}\psi_z)_z + \overline{\rho}\psi_{xx}]_{tt} + \overline{\rho}N^2\psi_{xx} = 0, \tag{5}$$

where $N^2(z) = -g\overline{\rho}_z/\overline{\rho}$ is the square of the buoyancy frequency. Note that, in several anelastic models, N^2 is defined instead by the vertical gradient of potential temperature or potential density. For more on these different definitions of N, see Sutherland (2010) and Eckermann et al. (1998).

Figure 1 shows the model setup. The region of the duct, $-h < z < h$, is labeled D and has variable $N^2(z)$. Region U above the duct has constant $N^2 = N_1^2$, and region L below the duct has constant $N^2 = N_2^2$. Two profiles for $N^2(z)$ are plotted in Fig. 1: $N_1^2 = N_2^2 = 0$, which we use as a test case, and $N_1^2 = N_2^2 = 0.1N_0^2$, which we use to simulate radiation from the duct. In the examples of this paper, $h = 5$ km, and $N(z)$ is defined by Eq. (44) with maximum value $N_0 = 2\pi/(2\,\text{min})$. This N_0 is relatively large for the mesosphere, about twice the maximum value in the numerical simulation of Snively and Pasko (2003) and in the data of Smith et al. (2003); however, it is the same N_0 used in the numerical simulations of Laughman et al. (2011), a study that we want to compare with closely in this initial analysis of the theoretical model.

Outside of the duct, the density is

$$\overline{\rho} = \rho_{1,2} \exp[-N_{1,2}^2(z \mp h)/g], \tag{6}$$

where $\mp$ refers to the regions U and L, respectively. Within the duct, $\overline{\rho}(z)$ varies continuously from ρ_2 at $z = -h$ to ρ_1 at $z = h$, with a stable stratification $\rho_1 < \rho_2$.

For this linearized problem, it is convenient to work in Fourier space. Thus, we seek a solution to Eq. (5) in the form $\psi(x, z, t) = \phi(z) \exp(ikx - i\omega t)$ so that

$$(\overline{\rho}\phi_z)_z - k^2\overline{\rho}\phi + \frac{\overline{\rho}N^2}{c^2}\phi = 0, \tag{7}$$

where $c = \omega/k$. This equation holds at all z. The boundary conditions are that either $\overline{\rho}^{1/2}\phi \to 0$ as $z \to \pm\infty$ or that the solution is an outgoing wave. Thus, the solution in region U is

$$\phi = A \exp[N_1^2(z - h)/2g] \exp[-\gamma_1(z - h)], \tag{8}$$

and the solution in region L is

$$\phi = mA \exp[N_2^2(z + h)/2g] \exp[\gamma_2(z + h)], \tag{9}$$

where m is a constant and

$$\gamma_{1,2}^2 = k^2 + \frac{N_{1,2}^4}{4g^2} - \frac{N_{1,2}^2}{c^2}. \tag{10}$$

Here, $\gamma_{1,2}$ is chosen so that $\gamma_{1,2} > 0$ when it is real valued or $kc\mathrm{Im}(\gamma_{1,2}) > 0$ when it is pure imaginary, corresponding to exponential decay or an outgoing wave, respectively. Note that, in the Boussinesq approximation, $N_{1,2}^2/g \to 0$.

In the duct,

$$\phi = A\phi_D(z) \quad \text{in} \quad -h < z < h, \tag{11}$$

where ϕ_D satisfies the full equation [Eq. (7)]. The modal function is normalized to unity so that $\phi_D(h) = 1$, and A is the amplitude at the upper boundary of the duct.

The solution is now completed by requiring that ϕ and ϕ_z are continuous at the boundaries between region U, region L, and the duct D. Continuity of ϕ at $z = h$ is already satisfied by the normalization condition, while continuity of ϕ at $z = -h$ gives $\phi_D(-h) = m$. Then continuity of ϕ_z yields

$$\phi_{Dz}(h) = -\gamma_1 + \frac{N_1^2}{2g}, \quad \phi_{Dz}(-h) = m\left(\gamma_2 + \frac{N_2^2}{2g}\right). \tag{12}$$

The boundary conditions at $z = h$ uniquely determine ϕ_D as a function of z, k, and c, and then the boundary conditions at $z = -h$ determine m and the dispersion relation expressing c in terms of k.

However, we are concerned with the limit $kh \to 0$. Hence, we introduce a small parameter ε such that $kh \sim \varepsilon$, but z/h in regions U and L scales as $1/\varepsilon$. We also suppose that the stratification in regions U and L is weak so that $N_{1,2}^2/N_0^2$ is $O(\varepsilon)$. It follows that $\gamma_{1,2}h$ is also $O(\varepsilon)$. Then we seek an expansion in ε, in which it will be sufficient to keep only the leading $O(\varepsilon)$ terms. It follows that, in the duct, the k^2 term in Eq. (7) can be omitted, and ϕ_D satisfies the long-wave modal equation,

$$(\overline{\rho}\phi_{Dz})_z + \frac{\overline{\rho}N^2}{c^2}\phi_D = 0 \quad \text{in} \quad -h < z < h. \tag{13}$$

Next, we write

$$\phi_D = \phi_D^{(0)} + \phi_D^{(1)} + \cdots, \quad c = c_0 + c_1 + \cdots, \tag{14}$$

where the terms with index 0 are of order unity, and the terms with index 1 are of order ε. At leading order, $\phi_D^{(0)}$ satisfies Eq. (13) with $c = c_0$ and the boundary conditions obtained from Eq. (12) at the leading order:

$$\phi_{Dz}^{(0)}(h) = \phi_{Dz}^{(0)}(-h) = 0. \tag{15}$$

The modal equation [Eq. (13)] and the boundary conditions in Eq. (15) determine an infinite set of linear long-wave modes with speeds c_0. Although the following analysis is valid for any one of these modes, in practice we take the lowest mode: that is, the one for which $\phi_D^{(0)}$ has just one zero in $-h < z < h$. Such a mode has $\phi_{Dz}^{(0)} > 0$ in the duct, and so, in particular, $m_0 = \phi_D^{(0)}(-h) < 0$. We call this a "mode 2" wave, as the amplitude has opposite signs on each side of the duct. Note that the boundary conditions [Eq. (15)] prohibit a "mode 1" wave with no internal zeros. Technically, such a mode does exist, but with $1/c_0 = 0$. It is pertinent to note that the vertical particle displacement $\eta = \psi/c_0$ at the leading order.

We now proceed to the next order, where the equation describing the first-order correction to $\phi_D^{(0)}$ is given by

$$(\overline{\rho}\phi_{Dz}^{(1)})_z + \frac{\overline{\rho}N^2}{c_0^2}\phi_D^{(1)} = \frac{2\overline{\rho}N^2c_1}{c_0^3}\phi_D^{(0)}, \tag{16}$$

which satisfies the upper-boundary conditions:

$$\phi_D^{(1)}(h) = 0, \quad \phi_{Dz}^{(1)}(h) = -\gamma_1 + \frac{N_1^2}{2g}. \tag{17}$$

Equation (16) with the boundary conditions in Eq. (17) determines $\phi_D^{(1)}$ uniquely. But from the boundary conditions in Eq. (12), we see that also

$$\phi_{\mathrm{D}z}^{(1)}(-h) = m_0\left(\gamma_2 + \frac{N_2^2}{2g}\right) \tag{18}$$

must hold, where $m_0 = \phi_{\mathrm{D}}^{(0)}(-h)$. Thus a compatibility condition is needed to determine c_1. This is obtained by multiplying Eq. (16) by $\phi_{\mathrm{D}}^{(0)}$ and integrating over D. On using the boundary conditions in Eqs. (15), (17), and (18), we find that

$$\frac{2c_1}{c_0} I = \rho_1\left(-\gamma_1 + \frac{N_1^2}{2g}\right) - \rho_2 m_0^2\left(\gamma_2 + \frac{N_2^2}{2g}\right), \tag{19}$$

where

$$I = \int_{\mathrm{D}} \overline{\rho}\frac{N^2}{c_0^2}\phi_{\mathrm{D}}^{(0)2}\, dz = \int_{\mathrm{D}} \overline{\rho}\phi_{\mathrm{D}z}^{(0)2}\, dz. \tag{20}$$

Equation (19) is the asymptotic ($kh \to 0$) outcome in Fourier space. To convert this to a partial differential equation in physical space, the first step is to rewrite Eq. (19) as an operator on the amplitude A defined in Eq. (11). This gives

$$c_1 A + M(k)A = 0, \tag{21}$$

where

$$\frac{2I}{c_0} M(k) = \rho_1\left(\gamma_1 - \frac{N_1^2}{2g}\right) + \rho_2 m_0^2\left(\gamma_2 + \frac{N_2^2}{2g}\right). \tag{22}$$

Note that, when $N_{1,2}^2 = 0$, $\gamma_{1,2} = |k|$ and $M(k) = \beta|k|$, where $2I\beta/c_0 = \rho_1 + m_0^2\rho_2$.

The second step is to recall that the full amplitude is $A_f = A\exp[ik(x - ct)]$; hence, we may replace ik with $\partial/\partial\xi$ and $-ikc_1$ with $\partial/\partial T$; here, $\xi = x - c_0 t$, and T is a slow time relative to the ξ reference frame. Then Eq. (21) becomes a linear differential operator acting on A_f. At this stage, we also add the nonlinear term into Eq. (21), readily found from the literature (e.g., Benjamin 1967; Davis and Acrivos 1967). The final outcome is the nonlinear evolution equation for the physical amplitude $A(\xi, T)$, where, for convenience, we now omit the subscript f to obtain

$$A_T + \alpha A A_\xi + \mathcal{M}(A_\xi) = 0. \tag{23}$$

Here,

$$\mathcal{M}(A) = -\frac{1}{2\pi}\int_{-\infty}^{\infty} M(k)\hat{A}\exp(ik\xi)\, dk, \tag{24}$$

and

$$\hat{A}(k, T) = \int_{-\infty}^{\infty} A(\xi, T)\exp(-ik\xi)\, d\xi \tag{25}$$

is the Fourier transform of A. The nonlinear coefficient is

$$\alpha = \frac{3}{2}\frac{\int_{\mathrm{D}} \overline{\rho}(\phi_{\mathrm{D}}')^3\, dz}{\int_{\mathrm{D}} \overline{\rho}(\phi_{\mathrm{D}}')^2\, dz}, \tag{26}$$

where we have now, and in the sequel, omitted the zero superscript. Note that, since the amplitude $A(\xi, T)$ is real valued, we can verify that $\mathcal{M}(A_\xi)$ is likewise real valued.

b. Decay estimates

In general, the model Eq. (23) can be integrated numerically using appropriate initial conditions (see section 3 below). When $N_{1,2}^2 = 0$, Eq. (23) reduces to the BDAO equation and has the solitary wave solution

$$A = \frac{a\lambda^2}{Y^2 + \lambda^2}, \quad Y = \xi - VT \tag{27}$$

with

$$V = \frac{\alpha a}{4} = \frac{\beta}{\lambda}. \tag{28}$$

There are also known periodic wave solutions and modulated periodic wave solutions describing an undular bore (Jorge et al. 1999). In particular, we note that the leading wave in an undular bore with an initial jump discontinuity D_0 is a solitary wave of amplitude $4D_0$. But when $N_{1,2}^2 \neq 0$, the solutions of Eq. (23) lose energy by radiation into regions U and L, as shown from the energy equation:

$$\frac{d}{dT}\int_{-\infty}^{\infty} A^2\, d\xi = \frac{1}{2\pi}\int_{-\infty}^{\infty} ikM(k)|\hat{A}|^2\, dk. \tag{29}$$

When $N_{1,2}^2 = 0$, $M(k) = \beta|k|$, and the integral on the right-hand side is zero. But when $N_{1,2}^2 \neq 0$, $\gamma_{1,2} = im_{1,2}\mathrm{sign}(k)$ for $|k| < k_{1,2}$ and vertical wavenumber $m_{1,2}$ in regions U and L respectively, where

$$k_{1,2}^2 = \frac{N_{1,2}^2}{c_0^2} - \frac{N_{1,2}^4}{4g^2}, \quad m_{1,2}^2 = k_{1,2}^2 - k^2. \tag{30}$$

Formally, $N_{1,2}^2$ are $O(\varepsilon)$ so that the first term for $k_{1,2}^2$ dominates. Then the energy equation [Eq. (29)] becomes

$$\frac{d}{dT}\int_{-\infty}^{\infty} A^2\, d\xi = \frac{-c_0}{2\pi I}\left(\rho_1\int_{-k_1}^{k_1} |km_1||\hat{A}|^2\, dk + \rho_2 m_0^2\int_{-k_2}^{k_2} |km_2||\hat{A}|^2\, dk\right). \tag{31}$$

Since the right-hand side is negative, this expression shows that energy is lost from the duct.

A simple estimate of the decay rate can be made for small $N_{1,2}^2$ by using the BDAO solitary wave to estimate A and $\hat{A}$ in Eq. (31). First,

$$\hat{A} = \pi a\lambda \exp(-\lambda|k|) \quad \text{and} \tag{32}$$

$$\int_{-\infty}^{\infty} A^2\, d\xi = \frac{1}{2\pi}\int_{-\infty}^{\infty} |\hat{A}^2|\, dk = \frac{\pi a^2\lambda}{2}. \tag{33}$$

Then, substituting into Eq. (31) and estimating the right-hand side for small $|kh|$ yields

$$\frac{da}{dt} = -\frac{8c_0\beta}{3I\alpha}(\rho_1 k_1^3 + \rho_2 m_0^2 k_2^3). \tag{34}$$

This is the initial linear decay rate found by Maslowe and Redekopp (1980), Pereira and Redekopp (1980), and Grimshaw (1981b). The full expression obtained by substituting Eqs. (32) and (33) into Eq. (34) is

$$\frac{da}{dt} = -\frac{8c_0\beta}{I\alpha}[\rho_1 k_1^3 F(2\lambda k_1) + \rho_2 m_0^2 k_2^3 F(2\lambda k_2)], \tag{35}$$

where

$$\lambda = \frac{4\beta}{\alpha a} \quad \text{and} \quad F(\chi) = \int_0^{\pi/2} \sin\theta\cos^2\theta \exp(-\chi\sin\theta)\, d\theta. \tag{36}$$

As $\chi \to 0$, $F \to 1/3$, and this agrees with Eq. (34). On the other hand, as $a \to 0$, $\chi \to \infty$, and $F \to 1/\chi^2$. In general, $F(\chi)$ can be expressed in terms of Bessel functions (Maslowe and Redekopp 1980). In these two limiting cases, respectively,

$$a_0 - a \sim \frac{8c_0\beta}{3I\alpha}(\rho_1 k_1^3 + \rho_2 m_0^2 k_2^3)t,$$
$$a \sim \frac{a_0}{1 + \Gamma a_0 t}, \quad \text{and} \quad \Gamma = \frac{c_0\alpha}{8I\beta}(\rho_1 k_1 + \rho_2 m_0^2 k_2). \tag{37}$$

This decay rate can also be used to estimate the decay rate of an undular bore, recalling that the leading wave in an undular bore of an initial jump discontinuity has an amplitude of $4D_0$ in the absence of any outward radiation. We note that Matsuno et al. (2007) have used the Whitham method to derive estimates for the decay of an undular bore under weak frictional effects, and that approach could conceivably also be used here.

It is useful to consider also the linear decay rate for a sinusoidal disturbance. That is, the linearized version of Eq. (23) has a solution:

$$A = A_0 \exp(iK\xi - i\Omega T) + \text{c. c.}, \quad \Omega = -KM(K). \tag{38}$$

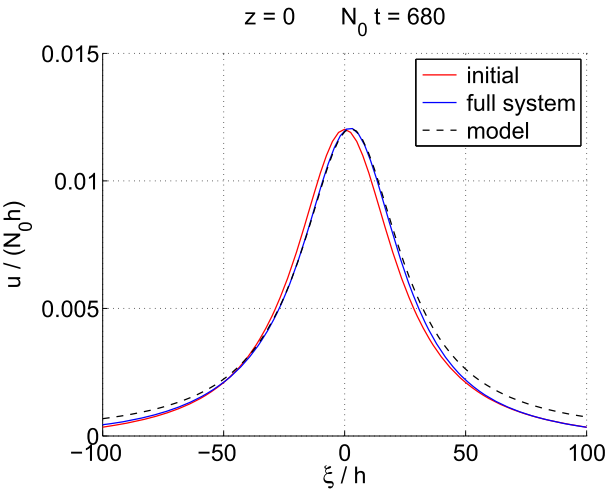

FIG. 2. Test case, using the duct parameters described in section 4 with $N_B = 0$ in Eq. (44). The initial vertical displacement amplitude is $\eta_0 \simeq 72$ m, and $\lambda = 25h = 125$ km. The plot shows only part of the computational domain, which has length $\xi/h = 2500$.

Thus, for $|K| > k_{1,2}$ the linear wave disperses with no amplitude decay, but, for $|K| < k_{1,2}$, the linear wave decays exponentially:

$$|A|^2 = A_0^2 \exp[2(\text{Im}\Omega)T]. \tag{39}$$

3. Numerical methods

We have carried out two sets of simulations. The first set is based on the model evolution equation [Eq. (23)], referred to herein as the "model," and the second set is based on the two-dimensional Navier–Stokes equations in the Boussinesq approximation, referred to herein as the "full system."

a. *Model evolution equation*

The model evolution equation [Eq. (23)] for $A(x, t)$ was solved using a standard spectral collocation method (Boyd 2001) with a Fourier series in x and a Runge–Kutta time step. The examples below were computed with 1024 grid points in x. The equations for the vertical dependence [i.e., Eq. (13) for $\phi_D^{(0)}(z)$ and c_0 and Eq. (16) for $\phi_D^{(1)}(z)$] were solved using a Chebyshev derivative matrix to approximate the vertical derivatives, with 81 grid points across the duct $|z| \le h$. The method was tested by comparing the results with the analytic solitary wave solution [Eq. (27)]; see Table 1 of Laughman et al. (2011) and Fig. 2 herein.

b. *Full system*

The full system is the Boussinesq two-dimensional Navier–Stokes equations used by Laughman et al. (2009,

2011) to model mesospheric bores. From Laughman et al. [2011, their Eq. (14)],

$$\mathbf{u}_t + (\mathbf{u}\cdot\nabla)\mathbf{u} = \nu\nabla^2\mathbf{u} - \nabla P/\overline{\rho}_0 - \hat{\mathbf{z}}g\rho/\overline{\rho}_0, \quad (40)$$

$$\theta_t + (\mathbf{u}\cdot\nabla)\theta = \kappa\nabla^2\theta, \quad (41)$$

$$\nabla\cdot\mathbf{u} = 0, \quad \text{and} \quad (42)$$

$$\rho = \overline{\rho}_0[1 - (\theta - \overline{\theta}_0)/\overline{\theta}_0]. \quad (43)$$

Here, $\mathbf{u} = (u, w)$ is the velocity vector, P is the pressure, ρ is the density, θ is the potential temperature, g is gravity, $\hat{\mathbf{z}}$ is the vertical unit vector, ν is the kinematic viscosity, and κ is the thermal diffusivity. The overbar indicates a background quantity, with the zero subscript for a representative value. We set $g = 9.55\,\mathrm{m\,s^{-2}}$ and $\overline{\theta}_0 = 8500\,\mathrm{K}$, appropriate for an altitude near 100 km. The simulations are effectively inviscid with $\kappa = \nu = 10^{-4}\,\mathrm{m^2\,s^{-1}}$. The background density and potential temperatures correspond to the specified profile for $N(z)$ given below in Eq. (44).

The full system is solved by a pseudospectral method (Spalart et al. 1991) with a third-order Runge–Kutta routine for the time step. The computational domain is periodic in x and has reflecting boundaries in z. The grid has 1000 points in x, 2500 points in z, and a time step of $6.8/N_0$, where N_0 is given in Eq. (44). The upper and lower boundaries are located at $z = \pm 25h$ for the BDAO initial condition and at $z = \pm 50h$ for the sinusoid initial condition. These initial conditions are described in section 3d.

c. Duct parameters

We use the same form for $N(z)$ as in Laughman et al. [2011, their Eq. (16b)]. Within the duct, $|z| \le h$, and

$$N^2(z) = N_B^2 + \frac{1}{2}(N_0^2 - N_B^2)[1 + \cos(\pi z/h)]. \quad (44)$$

The maximum value of N is $N_0 = N(z = 0)$. Outside the duct, $|z| > h$, and $N = N_B = N(z = \pm h)$. In the notation of section 2, $N_1 = N_2 = N_B$.

We set $N_0 \simeq 0.0524\,\mathrm{s^{-1}}$, corresponding to a buoyancy period of 2 min, and $h = 5\,\mathrm{km}$. In the following examples, $N_B^2 = 0.1N_0^2$, which gives $c_0 = 98\,\mathrm{m\,s^{-1}}$. For comparison, $N_B = 0$ gives $c_0 = 88.3\,\mathrm{m\,s^{-1}}$, and the BDAO solitary wave speed in the ξ reference frame $V = 0.98\,\mathrm{m\,s^{-1}}$, with V given by Eq. (28).

As noted in section 3d, the full-system initialization has an envelope function to ensure that the vertical velocity is zero at the upper and lower boundaries. For the BDAO initial condition, this led to some initial perturbations well outside the duct, which then radiated small-amplitude waves. To minimize this radiation, we set $N^2 = 0$ in the top and bottom half of the domain for the case of the BDAO initial condition. Although these $N^2 = 0$ layers reflect waves propagating away from the duct (see Fig. 4 discussed below), they were useful in vertically isolating the effects of the initial perturbation in these outer regions.

d. Initial conditions

Two initial conditions are considered: the BDAO solitary wave equation [Eq. (27)], and a sinusoidal wave in x. The former has initial vertical displacement [Laughman et al. (2011), their Eq. (17a)]:

$$\eta(x,z) = \begin{cases} \dfrac{\eta_0\lambda^2}{x^2+\lambda^2}\phi_{\mathrm{D}}^{(0)}(z), & |z| \le h \\ \mathrm{sign}(z)\dfrac{\eta_0(\lambda + |z| - h)^2}{x^2 + (\lambda + |z| - h)^2}E(z), & |z| > h \end{cases}. \quad (45)$$

Here, $\phi_{\mathrm{D}}^{(0)}(z)$ is the lowest vertical mode computed from Eq. (13), and $E(z)$ is an envelope function to ensure that $w = 0$ at the upper and lower boundaries ($z = \pm z_m$):

$$E(z) = \frac{1}{2}\{\tanh[(z + z_m/4)/h] - \tanh[(z - z_m/4)/h]\}. \quad (46)$$

The sinusoidal initial condition is [Laughman et al. (2011), their Eq. (19a)]

$$\eta(x,z) = \begin{cases} \eta_0 \sin(2\pi x/\lambda_x)\phi_{\mathrm{D}}^{(0)}(z), & |z| \le h \\ \mathrm{sign}(z)\eta_0 \sin(2\pi x/\lambda_x)E(z) \times \exp[-2\pi(|z| - h)/\lambda_x], & |z| > h \end{cases}. \quad (47)$$

The initialization of the full system is described by Laughman et al. (2011) and is followed here. For instance, the initial vertical velocity is $w = -c_b\eta_x$ for the solitary wave initialization equation [Eq. (45)], where $c_b = V + c_0$ is the BDAO solitary wave speed, with V given in Eq. (28); and $w = -c_0\eta_x$ for the sinusoidal initial condition [Eq. (47)]. More details on the initialization are given in Laughman et al. (2011).

The model equation [Eq. (23)] requires only the initialization of $A(x, t)$, related to the streamfunction by $\psi = A(x, t)\phi(z)$. The radiated waves outside the duct are

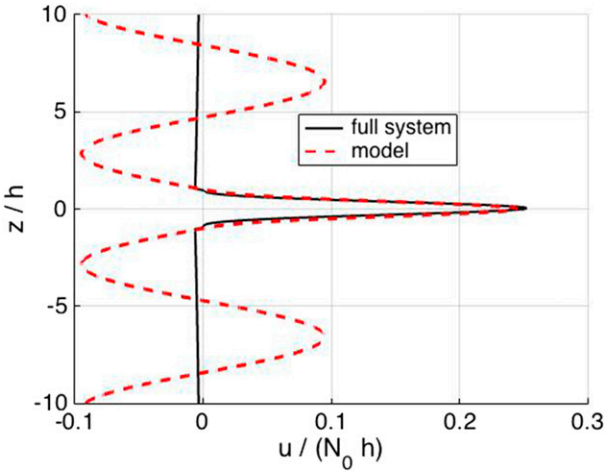

FIG. 3. The initial horizontal velocity $u(x = 0, z)/(N_0 h)$ in the full-system equations (solid black) and in the model equation (red dashed) for the sinusoid initial condition.

automatically included in the initial condition and at later times through Eqs. (8) and (9).

Figure 3 shows the initial condition for $u(x = 0, z)$ in the full system (solid black curve) and in the model (red dashed curve). This is for the sinusoidal initialization. Both the model and the full system have a mode-2 vertical structure inside the duct, proportional to ϕ_z, as discussed below Eq. (15). Only the model has the radiated waves outside the duct. For the full system, u is close to zero at the duct boundaries $z = \pm h$ and is gradually decreased to zero with increasing distance from the duct.

We have already noted that A is required to be real valued. However, when deriving the linearized part of the model equation [Eq. (7)], A was the amplitude of the Fourier component $\exp(ikx - i\omega t)$. For example, in the upper region U, using Eq. (8) in the Boussinesq approximation,

$$\psi(x, z, t) = A \ \exp(ikx - i\omega t) \exp[-\gamma_1(z - h)]. \qquad (48)$$

When this Fourier component corresponds to a propagating wave in region U, then γ_1 is imaginary, and the phase of ψ in region U is $kx - \omega t - m_1(z - h)$, where m_1 is the vertical wavenumber [see Eq. (30)]. For a general initial condition, for example the solitary wave [Eq. (27)], we still need to associate a complex function with the real-valued A to obtain the proper phase for propagation in regions U and L. The way we do this involves the Hilbert transform $H(A)$ (Hahn 1996), applied in the x direction, where this is defined by its Fourier transform $\widehat{H(A)} = -i\hat{A}\,\mathrm{sign}(k)$, with $\hat{A}$ as the Fourier transform of A defined by Eq. (25). In region U, we write,

$$\psi(x, z, t) = [A + iH(A)] \exp[-\gamma_1(z - h)]. \qquad (49)$$

For the special case of $A = \cos(kx - \omega t)$, then $H(A) = \sin(kx - \omega t)$, and we recover Eq. (48) (with $A = 1$). The complex form $A + iH(A)$ is equivalent to the one-sided Fourier integral

$$A + iH(A) = \frac{1}{\pi} \int_0^\infty \hat{A}(k, t) \exp(ikx)\, dk. \qquad (50)$$

So the generalization of the case of a single Fourier component is to associate $\exp(ikx)$ with the corresponding Fourier component $\hat{A}(k, t)$ and to obtain the time dependence from Eq. (23). Within the duct,

$$\psi(x, z, t) = [A + \imath H(A)](\phi_D^{(0)} + \phi_D^{(1)}). \qquad (51)$$

The term $\phi_D^{(1)}$ is significant for the value of N_B used in the following numerical results.

The computational procedure is to integrate the model equation [Eq. (23)] numerically for $A(x, t)$, then take its Hilbert transform at each time step to compute $\psi(x, z, t)$ from Eq. (51) in the duct, from Eq. (49) in region U, and from a corresponding equation in region L. Note that, for $N_1 = N_2 = 0$, the Hilbert transform term is not needed, because $\phi_D^{(1)}$ and $\gamma_{1,2}$ are then real valued, in addition to $\phi_D^{(0)}$ and A, which are always real valued.

4. Numerical results

First, we show the case where the initial condition is the BDAO solitary wave equation [Eq. (45)] with $\lambda = 25h$. A typical result is plotted in Figs. 4 and 5. Both the model and full-system simulations show that the wave decays by radiation out of the duct, and the decay rates are shown in Fig. 6.

Overall, there is very good agreement with the theoretical predictions from the BDAO model and between the model and full-system simulations. One difference is in the transients generated in the full system and seen in Fig. 5 at $\xi/h \sim 500$ and -750. These are presumably present because of the adjustment of the initial condition to the actual solitary wave structure and the radiated waves from the duct. Laughman et al. (2011) show similar transients, which, in part, result from a mismatch between the initial temperature and vertical velocity fields and seem to propagate at linear wave speeds.

For the full system in Fig. 4, there is wave reflection evident at the top and bottom of the plot, near $\xi/h \simeq 50$. The reflected waves return to the duct region and contribute to the local maximum in the duct near $\xi/h \simeq 140$. This reflection is from the $N^2 = 0$ layers mentioned at the end of section 3c. Experiments with larger domains

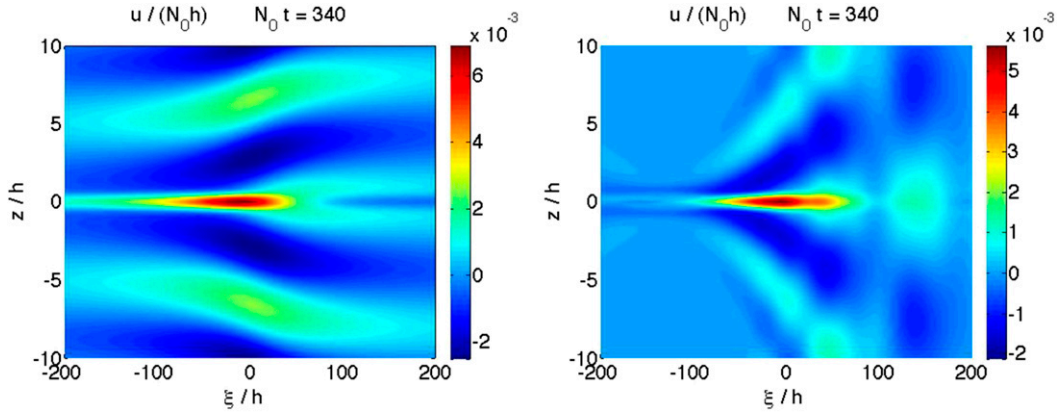

FIG. 4. Solutions for $u/(N_0h)$ using the BDAO solitary wave initial condition [Eq. (45)] with $\lambda = 25h$: (left) the model and (right) the full system.

indicate that the reflected waves do not affect the maximum amplitude of the main solitary wave in the duct.

Figure 6 shows that the amplitude in the full system initially increases by a small amount before following the same decay rate as that for the model and as predicted theoretically. This initial small increase is part of the response to the initial conditions, though the exact reason in unclear. It also occurs for the sinusoid initial condition (see Fig. 9, discussed below). An initial increase is suggested by the theory of Grimshaw (1981c), which contains higher-order terms that are not included in our theoretical model.

The maximum value for $u/(N_0h)$ in Fig. 4 is about 6×10^{-3}, corresponding to $u \simeq 1.6\,\mathrm{m\,s^{-1}}$. The time $N_0t = 340$ corresponds to $t = 108\,\mathrm{min}$.

We next show the case when the initial condition is a sinusoidal wave [Eq. (47)]. A typical result is plotted in Figs. 7 and 8, which show the formation of an undular bore, albeit decaying because of radiation. Indeed, the effect of the radiation is to prevent the formation of rank-ordered waves in the undular bore, since, as the leading larger waves form, so do they begin to decay. We note that a similar simulation for a smaller initial amplitude, one-third of that shown in Fig. 7, did not show the formation of an undular bore and instead dispersed and decayed essentially by linear dynamics in both the full system and the model. Laughman et al. (2011, section 4.3) discuss the full-system solutions for other initial sinusoid amplitudes and other values of N_B.

The bore waves in Fig. 7 have a horizontal wavelength of about $5h = 25\,\mathrm{km}$ and a peak value for $u/(N_0h)$ of

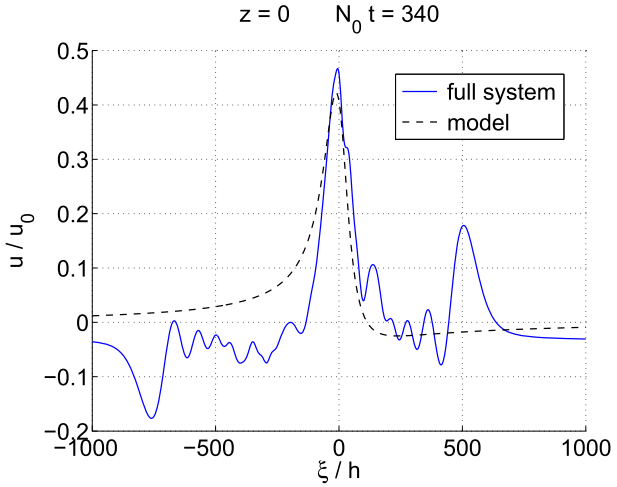

FIG. 5. Cross section at $z = 0$ of the solutions shown in Fig. 4. The solutions are normalized by the peak amplitude u_0 at $t = 0$.

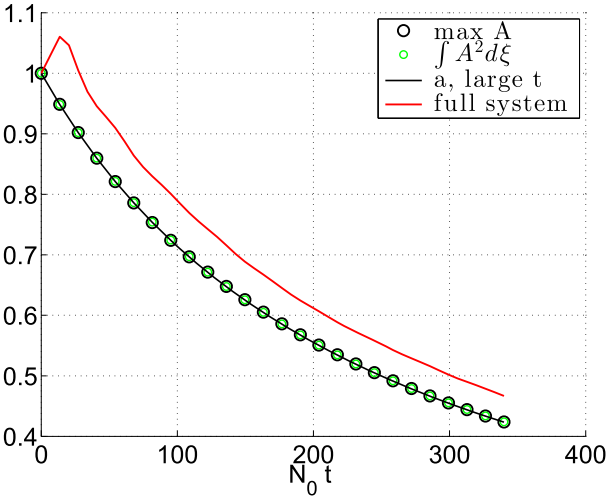

FIG. 6. Decay rates for the solutions shown in Fig. 4. For the model, we show both a local measure max(A) and an integrated measure, $\int A^2\,d\xi$; for the full system, we show only the local measure. The theoretical decay rate (solid blue) is obtained from the large time limit case of Eq. (37).

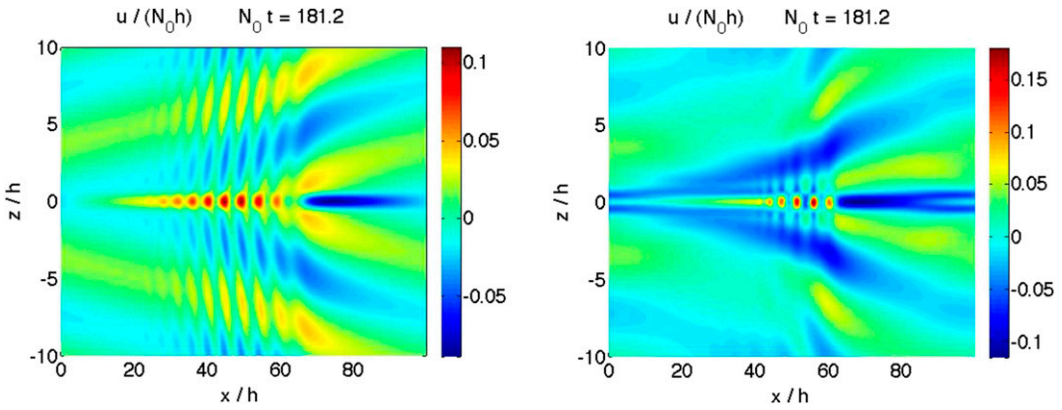

FIG. 7. Solutions using the sinusoidal wave initial condition [Eq. (47)] with $\lambda_x = 100h$ and $\eta_0 = 0.3h$: (left) the model and (right) the full system.

about 0.15, corresponding to $u \simeq 40\,\mathrm{m\,s^{-1}}$. The time $N_0 t = 181$ corresponds to $t = 58$ min.

The decay rates are shown in Fig. 9 based on both the maximum amplitude and an integrated measure of the disturbance amplitude. For the model simulations, we see initially that the sinusoidal disturbance decays linearly according to the decay law [Eq. (39)], but when the undular bore begins to form around $N_0 t = 80$, the leading solitary waves then decay according to the solitary wave decay rate [Eq. (37)], where we have used the large time limit. Note that the solitary wave decay is best measured here by the maximum amplitude, while the integrated measure $(\int A^2\, d\xi)^{1/2}$ measures the overall disturbance and follows the linear decay law for the initial disturbance wavelength.

In contrast, for the full system, the same decay rates are rather variable. After an initial adjustment in amplitude, the early stages do exhibit evidence of sinusoidal decay until $N_0 t \sim 100$. After this time, the variability of the decay rate is largely due to the rigid and reflecting upper and lower boundaries in the full system, which trap the wave energy within the domain. Wave energy radiated away from the duct thus eventually returns to the duct region. Plots of the time evolution of the solution (not shown) indicate that much of the reflection is associated with the long wavelengths of the initial sinusoid. Simulations with the sine-wave initial condition were also performed (not shown) using values of N_B^2 much smaller than the value of $0.1N_0^2$ in the present examples. For these simulations, there was less radiation away from the duct, and the decay rates for the model and the full system were more closely matched. The full-system solutions for these smaller values of N_B are discussed in Laughman et al. (2011, section 4.3).

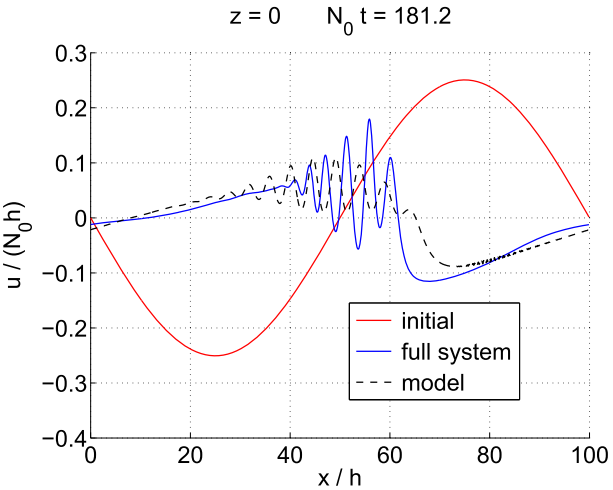

FIG. 8. Cross section at $z = 0$ of the solutions shown in Fig. 7.

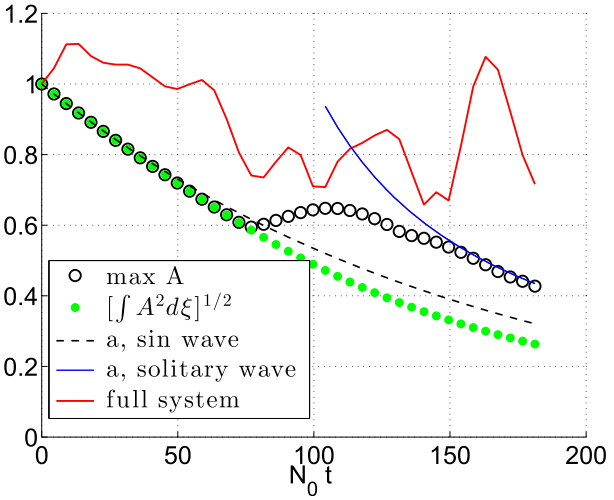

FIG. 9. Decay rates for the solutions shown in Fig. 7. The theoretical linear decay rate (dashed) is that estimated from Eq. (39), and the theoretical solitary wave decay rate (solid blue) is that estimated from the large time limit of Eq. (37).

Figures 7 and 8 show that, compared to the model solution, the full-system solution has larger trapped waves inside the duct (by a factor of about 2 in Fig. 8) and smaller radiated waves outside the duct, particularly at the short scales of the developing bore. This difference persists for longer times [$N_0 t = 453$ in Laughman et al. (2011, Fig. 13)]. Note that the short-scale radiated waves have high frequency, as revealed by the almost vertical slope of the phase lines outside the duct in the model solution of Fig. 7. The results may be somewhat sensitive to the differences in the high-frequency content of the full-system and model solutions, which affects the amount of trapping.

5. Discussion and conclusions

In this work, we have extended the weakly nonlinear BDAO model of a mesospheric duct described by Laughman et al. (2009, 2011) to include weak stratification in the adjoining deep layers. This then allows for internal gravity waves to be emitted from the duct by the nonlinear waves propagating along the duct. We have considered both the case when essentially a single solitary wave forms in the duct and a sinusoidal initial condition, which leads to the formation of an undular bore in the duct. In both cases, the nonlinear waves in the duct decay by radiation, in good agreement with the theoretical predictions from our extended BDAO model. The model results were compared with analogous simulations of the fully nonlinear system, and there is good overall agreement with the model. The large discrepancy between the model and the full-system decay rate shown in Fig. 9 is due in part to the reflection of the radiated waves from the rigid upper and lower boundaries of the computational domain in the full system. This highlights the value of an analytic model capable of properly handling the waves radiated from the duct and the need for a full-system model with radiation boundary conditions.

Our main conclusion is that, while nonlinear solitary waves can form in the duct, and although they do decay by radiation, they can survive as significant structures over sufficiently long periods so as to be observable. For the results presented here, our calculations indicate that the generated waves remain significant for $N_0 t > 300$, where $N_0 = 0.0524\,\mathrm{s}^{-1}$ is the maximum buoyancy frequency. That is, for the simulations reported here, the waves survive for at least $t > 95$ min, which certainly allows them to be observable. For example, Fig. 4 of Nielsen et al. (2006) displays the evolution of an observed mesospheric bore over a time period of 90 min with horizontal wavelength of about 20–30 km, similar to the bore wavelength shown here in Fig. 7.

Our main interest has been in the investigation of how weak stratification outside the duct affects the nonlinear waves in the duct. But we also considered a generic sinusoidal initial condition and demonstrated that this deformed into an undular bore, the leading waves of which become solitary waves and then decay by radiation. The more general issue of the energy source for the nonlinear waves and undular bores that can propagate in the duct remains for future work, but it has been suggested that a likely candidate could be vertically propagating gravity waves generated in the troposphere, which become trapped and break in the duct, generating a mixed region source for the horizontally propagating duct waves (e.g., Snively and Pasko 2003).

Acknowledgments. SDE was supported by the Chief of Naval Research through the Naval Research Laboratory's base 6.1 research program. We acknowledge Dr. Joseph Werne as the primary architect of the NWRA triple code described as the "full system" in section 3b. Funding for BL was provided by NSF grant AGS-1242943.

REFERENCES

Bageston, J. V., C. M. Wrasse, P. P. Batista, R. E. Hibbins, D. C. Fritts, D. Gobbi, and V. F. Andrioli, 2011: Observation of a mesospheric front in a thermal-doppler duct over King George Island, Antarctica. *Atmos. Chem. Phys.*, **11**, 12 137–12 147, doi:10.5194/acp-11-12137-2011.

Benjamin, T. B., 1967: Internal waves of permanent form in fluids of great depth. *J. Fluid Mech.*, **29**, 559–592, doi:10.1017/S002211206700103X.

Boyd, J. P., 2001: *Chebyshev and Fourier Spectral Methods.* 2nd ed. Dover, 688 pp.

Davis, R. E., and A. Acrivos, 1967: Solitary internal waves in deep water. *J. Fluid Mech.*, **29**, 593–607, doi:10.1017/S0022112067001041.

Dewan, E. M., and R. H. Picard, 1998: Mesospheric bores. *J. Geophys. Res.*, **103**, 6295–6305, doi:10.1029/97JD02498.

——, and ——, 2001: On the origin of mesospheric bores. *J. Geophys. Res.*, **106**, 6295–6305, doi:10.1029/2000JD900697.

Durran, D. R., and A. Arakawa, 2007: Generalizing the Boussinesq approximation to stratified compressible flow. *C. R. Mec.*, **335**, 655–664, doi:10.1016/j.crme.2007.08.010.

Eckermann, S. D., D. E. Gibson-Wilde, and J. T. Bacmeister, 1998: Gravity wave perturbations of minor constituents: A parcel advection methodology. *J. Atmos. Sci.*, **55**, 3521–3539, doi:10.1175/1520-0469(1998)055<3521:GWPOMC>2.0.CO;2.

Fechine, J., and Coauthors, 2009: First observation of an undular mesospheric bore in a Doppler duct. *Ann. Geophys.*, **27**, 1399–1406, doi:10.5194/angeo-27-1399-2009.

Grimshaw, R., 1981a: Evolution equations for long nonlinear internal waves in stratified shear flows. *Stud. Appl. Math.*, **65**, 159–188.

——, 1981b: Solitary waves in a compressible fluid. *Pure Appl. Geophys.*, **119**, 780–797, doi:10.1007/BF01131255.

——, 1981c: A second-order theory for solitary waves in deep fluids. *Phys. Fluids*, **24**, 1611–1618, doi:10.1063/1.863583.

Hahn, S. F., 1996: *Hilbert Transforms in Signal Processing.* Artech House, 460 pp.

Jorge, M. C., A. A. Minzoni, and N. F. Smyth, 1999: Modulation solutions for the Benjamin–Ono equation. *Physica D*, **132**, 1–18, doi:10.1016/S0167-2789(99)00039-1.

Laughman, B., D. C. Fritts, and J. Werne, 2009: Numerical simulation of bore generation and morphology in thermal and Doppler ducts. *Ann. Geophys.*, **27**, 511–523, doi:10.5194/angeo-27-511-2009.

——, ——, and ——, 2011: Comparisons of predicted bore evolutions by the Benjamin–Davis–Ono and Navier–Stokes equations for idealized mesopause thermal ducts. *J. Geophys. Res.*, **116**, D02120, doi:10.1029/2010JD014409.

Li, Q., J. Xu, J. Yue, X. Liu, W. Yuan, B. Ning, S. Guan, and J. P. Younger, 2013: Investigation of a mesospheric bore event over northern China. *Ann. Geophys.*, **31**, 409–418, doi:10.5194/angeo-31-409-2013.

Maslowe, S. A., and L. G. Redekopp, 1980: Long nonlinear waves in stratified shear flows. *J. Fluid Mech.*, **101**, 321–348, doi:10.1017/S0022112080001681.

Matsuno, Y., V. S. Shchesnovich, A. M. Kamchatnov, and R. A. Kraenkel, 2007: Whitham method for the Benjamin–Ono–Burgers equation and dispersive shocks. *Phys. Rev. E*, **75**, 016307, doi:10.1103/PhysRevE.75.016307.

Nielsen, K., M. J. Taylor, R. G. Stockwell, and M. J. Jarvis, 2006: An unusual mesospheric bore event observed at high latitudes over Antarctica. *Geophys. Res. Lett.*, **33**, L07803, doi:10.1029/2005GL025649.

Pereira, N. R., and L. G. Redekopp, 1980: Radiation damping of long, finite-amplitude internal waves. *Phys. Fluids*, **23**, 2182, doi:10.1063/1.862913.

Rottman, J. W., and R. Grimshaw, 2001: Atmospheric internal solitary waves. *Environmental Stratified Flows*, R. Grimshaw, Ed., Topics in Environmental Fluid Mechanics, Vol. 3, Kluwer, 61–88, doi:10.1007/0-306-48024-7_3.

Seyler, C. E., 2005: Internal waves and undular bores in mesospheric inversion layers. *J. Geophys. Res.*, **110**, D09S05, doi:10.1029/2004JD004685.

She, C. Y., T. Li, B. P. Williams, and T. Yuan, 2004: Concurrent OH imager and sodium temperature/wind lidar observation of a mesopause region undular bore event over Fort Collins/Platteville, Colorado. *J. Geophys. Res.*, **109**, D22107, doi:10.1029/2004JD004742.

Smith, R. K., 1988: Traveling waves and bores in the lower atmosphere: The ''Morning Glory'' and related phenomena. *Earth-Sci. Rev.*, **25**, 267–290, doi:10.1016/0012-8252(88)90069-4.

Smith, S. M., M. J. Taylor, G. R. Swenson, C. Y. She, W. Hocking, J. Baumgardner, and M. Mendillo, 2003: A multidiagnostic investigation of the mesospheric bore phenomenon. *J. Geophys. Res.*, **108**, 1083, doi:10.1029/2002JA009500.

Snively, J., and V. P. Pasko, 2003: Breaking of thunderstorm-generated gravity waves as a source of short-period ducted waves at mesopause altitudes. *Geophys. Res. Lett.*, **30**, 2254, doi:10.1029/2003GL018436.

——, ——, M. Taylor, and W. Hocking, 2007: Doppler ducting of short-period gravity waves by midlatitude tidal wind structure. *J. Geophys. Res.*, **112**, A03304, doi:10.1029/2006JA011895.

Spalart, P. R., R. D. Moser, and M. M. Rogers, 1991: Spectral methods for the Navier–Stokes equations with one infinite and two periodic directions. *J. Comput. Phys.*, **96**, 297–324, doi:10.1016/0021-9991(91)90238-G.

Stockwell, R. G., M. J. Taylor, K. K. Nielsen, and M. J. Jarvis, 2011: The evolution of a breaking mesospheric bore wave packet. *J. Geophys. Res.*, **116**, D19102, doi:10.1029/2010JD015321.

Sutherland, B. R., 2010: *Internal Gravity Waves.* Cambridge University Press, 377 pp.

Taylor, M. J., D. N. Turnbull, and R. P. Lowe, 1995: Spectrometric and imaging measurements of a spectacular gravity wave event observed during the ALOHA-93 Campaign. *Geophys. Res. Lett.*, **22**, 2848–2852, doi:10.1029/95GL02948.

Vallis, G., 2006: *Atmospheric and Oceanic Fluid Dynamics.* Cambridge University Press, 745 pp.